A Generalized Two-Dimensional Coupled-Mode Analysis of Curved and Chirped Periodic Structures in Open Dielectric Waveguides

ZONG-QI LIN, SHU-TONG ZHOU, WILLIAM S. C. CHANG, FELLOW, IEEE, SIAMAK FOROUHAR, MEMBER, IEEE, AND JEAN-MARC DELAVAUX, MEMBER, IEEE

Abstract—**A generalized two-dimensional coupled mode analysis of curved and chirped quasi-periodic structures in planar dielectric waveguides has been formulated. This analysis can be used to design curved and chirped quasi-periodic structures for obtaining phase matched interaction between two specific guided-wave beams. Alternatively, it can be used to calculate the amplitude and the phase of the diffracted guided-wave beam for a given quasi-periodic structure and for a specific incident beam, including the effect of the phase mismatch. The numerical example of linear chirped grating lenses with $F=10, f=20$ mm, $\Lambda_{min}=2$ μm, $\Lambda_{max}=4.1$ μm, and grating grooved length $=65$ μm is presented.**

I. Introduction

CURVED and chirped gratings in optical dielectric waveguides have been investigated by a number of researchers to obtain reflection, focusing, collimation, coupling, and Fourier analysis of guided waves [1]–[4]. These gratings will also be useful for millimeter-wave applications since similar dielectric wave guides are used in that region. In the past, most of these components are used to obtain coupling to radiation modes and reflection of guided waves by phase matched interactions. Recently, there developed a very strong interest in the use of chirped grating structures for transforming one form of guided-wave beam into another form of guided-wave beam. A typical example, a chirped grating lens, is illustrated in Fig. 1. In this case, the planar guided-wave beam has been diffracted into a focused guided-wave beam with an experimental efficiency of 90 percent [2]. Chirped grating lenses are important to integrated optics and guided-wave optical signal processing because of two reasons: 1) they are wavelength selective; and 2) they can be batch-fabricated. However, there is a lack of theoretical analysis that will assess the effect of the variation of grating patterns, that will establish their performance limitations, and that will allow us to optimize the design for different applications.

In guided-wave optics, chirped gratings are usually fabricated by processes such as electron-beam lithography or optical holographic exposure methods followed by etching or lift-off of the deposited film. There are severe limitations in the grating groove patterns that can be generated by these methods. For example, curved lines are usually approximated by linear line segments. The chirping rate and the curvature of the fabricated grating may be different than the designed pattern. Even for perfectly fabricated gratings, the phase matching conditions may be violated where either the angle of incidence or the shape of the input beam is deviated from its ideal alignment. For many other applications such as a guided-wave chirped grating analyzing lens in the RF spectrum analyzer, it is necessary to optimize the diffraction pattern of the lens for a range of incident angle of divergence and beam shape. In some cases, a chirped grating lens consisting of parallel grooves with varying periodicity where the phase matching condition is only partially satisfied is actually more advantageous to use than a curved grating. Therefore, the theoretical analysis for a chirped grating analysis must be able to take into account the effect of phase mismatch as well as the effect of curved guided-wave front and curved grating grooves.

The chirped grating structure that we shall analyze here is different from the chirped grating output coupler analyzed by Katzir *et al.* [5]. In Katzir's case, they were primarily interested in the coupling of a guided wave to the radiation modes. Here, we are only interested in the diffraction of a guided-wave beam into another guided-wave beam. The physical difference between the two cases is the periodicity Λ of the grating. In our case, the Λ values are sufficiently large and the $\boldsymbol{K}$ vector ($\boldsymbol{K}=2\pi/\Lambda$) is oriented in such a direction that only the diffracted guided-wave beam can satisfy approximately the phase matching condition. The substrate and air radiation modes will not be excited (except by scattering from random defects) because the phase mismatch for those modes is too large. Accord-

Manuscript received December 16, 1980; revised May 12, 1981. This work was supported in part by the Air Force Office of Scientific Research under Grant AFOSR 80-0037 to the University of California at San Diego.

Z.-Q. Lin and S.-T. Zhou are Visiting Scholars from the People's Republic of China. They are currently with the Department of Electrical Engineering and Computer Sciences, University of California at San Diego, La Jolla, CA 92093.

W. S. C. Chang, S. Forouhar, and J.-M. Delavaux are with the Department of Electrical Engineering and Computer Sciences, University of California at San Diego, La Jolla, CA 92093.

0018-9480/81/0800-0881$00.75 ©1981 IEEE

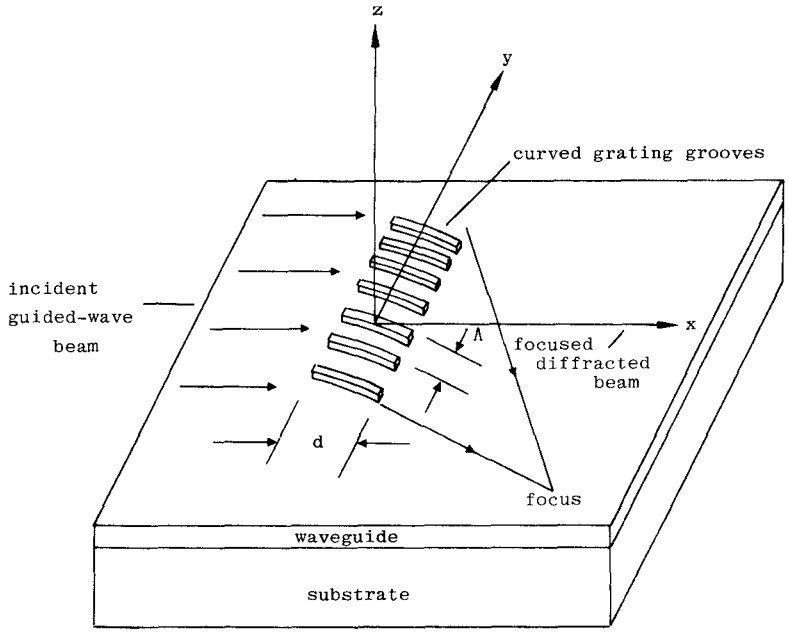

Fig. 1. Illustration of a curved chirped grating waveguide lens.

ing to Yao [6], this assumption is valid for a limited range of angles from the Bragg angle, e.g., 7° or 8° for a $LiNbO_3$ waveguide.

Analyses of the chirped and curved gratings have also been made by several other researchers. Hardy and Streifer [7] analyzed the focusing of a guided-wave Gaussian beam by a curved grating reflector. Solymar [8] presented a two-dimensional scalar wave theory of diffraction in volume holograms under the phase matched condition. In those two papers, the effect of phase mismatch was not discussed. Van Roey and Lagasse [9] discussed the analysis of a guided wave with Gaussian intensity distribution obliquely incident on a set of straight parallel-line grating grooves with constant periodicity, resulting in a plane diffracted beam. They considered the effect of phase mismatch. However, the coupled-mode equations for the plane guided-wave Fourier components are valid only for gratings with constant periodicity, thus, their analyses is not applicable to curved grating grooves.

In this paper, we have extended Solymar's theory to vector wave equations in the waveguide. The incident and diffracted guided waves are allowed to have curved wave fronts. An explicit procedure is given on how to determine the Eikonal lines for curved grating grooves and guided wave fronts. Following the work of Kogelnik [10], we have also formulated our analysis so that it can take into account a limited amount of phase mismatch by a dephasing term in the generalized two-dimensional coupled-mode theory. The limit of the validity within which dephasing can be handled by this method will be discussed in Section VI.

Following Kenan [11], we will assume that the planar waveguide supports only one discrete mode. The coupling to the radiation mode can be neglected when the propagation wavenumber of those radiation modes are substantially mismatched from the range of the propagation wave vectors of the incident beam and the grating $\boldsymbol{K}$ vectors. In other words, we assume that there are only two guided-wave beams coupled to each other via the chirped or curved grating structure. These two beams can have a variety of horizontal variations such as plane, cylindrical, or Gaussian beams, but their z variation is always given by the mode profile of the planar waveguide. The grating will have a localized orientation and periodicity, i.e., $\boldsymbol{\Lambda}$. The $\boldsymbol{\Lambda}$ varies slowly from one localized region of the grating to another. Within a localized region, the Bragg condition of diffraction is partially fulfilled by the $\boldsymbol{\Lambda}$ and two plane guided-waves representing the portion of the two beams in that localized region. The Q factor (given by $2\pi\lambda_e d/\Lambda^2$ for plane guided-waves where λ_e is the effective wavelength of the guided-wave mode and d is the length of volume interaction) is high enough so that diffractions by the grating grooves into other guided-wave beams can be neglected. Our approach is to substitute an assumed form of the two guided-wave beams (with unspecified amplitude and phase variations) into the vector wave equation. When a generalized phase matching condition is satisfied, the vector wave equation is reduced to a coupled two-dimensional differential equation relating the amplitude and phase variations of the two beams. The solutions of the coupled differential equations plus boundary conditions are obtained numerically on a digital computer to give the amplitude and phase variations of the two beams as they emerge from the grating region. In the following sections, we will discuss the derivation of the two-dimensional coupled differential equations, the numerical solutions of the coupled differential equations by means of the mesh points along Eikonal lines and the numerical results obtained for a few practical examples.

II. Formulation of the Generalized Coupled-Mode Analysis

The vector wave equation that we want to solve is

$$-\nabla\times\nabla\times\boldsymbol{E}+k_0^2\epsilon\boldsymbol{E}=0 \tag{1}$$

where we have assumed a exp ($j\omega t$) time variation, and k_0 is the free-space wavenumber ($k_0 = 2\pi/\lambda$).

A. The Generalized TE and TM Modes Without the Grating

For a lossless isotropic single mode planar waveguide, shown in Fig. 1, without any grating structure, we can express the total electric and magnetic field of the guided modes as a summation of the fields of generalized TE or TM guided-wave modes that have a z variation given by $F(z)$ multiplied by a function of x and y for each mode that describes the horizontal variation of that mode. Following the conventional analysis of the planar waveguide, let $F_E(z)$ be a TE eigenfunction of the ordinary differential equation

$$\left(\frac{\partial^2}{\partial z^2} + k_0^2\epsilon(z) - k_0^2 n_e^2\right) F_E(z) = 0 \tag{2}$$

with the conventional boundary conditions that both the tangential electric and magnetic fields must be continuous at all the dielectric interfaces. $\epsilon(z)$ is the relative dielectric constant of the waveguide and n_e is the eigenvalue representing the effective index of the guided-wave mode. The electric and magnetic field of the generalized TE mode is

$$\boldsymbol{E}_E(x, y, z) = [\nabla \times (\psi(x, y)\boldsymbol{i}_z)] F_E \tag{3a}$$

$$\boldsymbol{H}_E(x, y, z) = \frac{j}{\omega\mu_0\mu} \nabla \times \boldsymbol{E}_E \tag{3b}$$

where ψ is a solution of the following differential equation, representing the horizontal variation of the generalized TE guided-wave mode

$$\left(\frac{\partial^2}{\partial x^2} + \frac{\partial^2}{\partial y^2} + k_0^2 n_e^2\right) \psi(x, y) = 0. \tag{4}$$

Similarly, for the generalized TM mode, $F_M(z)$ is an eigenfunction of the differential equation

$$\frac{d}{dz}\left[\frac{1}{\epsilon(z)} \frac{d}{dz} F_M(z)\right] + \left[k_0^2 - \frac{k_0^2 n_e^2}{\epsilon(z)}\right] F_M(z) = 0 \tag{5}$$

with

$$\boldsymbol{H}_M(x, y, z) = [\nabla \times (\psi \boldsymbol{i}_z)] F_M \tag{6a}$$

$$\boldsymbol{E}_M(x, y, z) = \frac{-j}{\omega\epsilon_0\epsilon(z)} \nabla \times \boldsymbol{H}_M. \tag{6b}$$

For the TM modes, ψ is also a solution of (4).

When ψ takes the form $A \exp[-jk_0 n_e(\cos\theta x + \sin\theta y)]$, we obtain the usual TE or TM plane guided-wave beam propagating in a direction θ from the x axis. In general, when the size of the guided-wave beam is much larger than the wavelength, we can write the generalized guided-wave beam in the Sommerfeld–Runge form [12]

$$\psi(x, y) = A(x, y) \exp[-jk_0 n_e \phi(x, y)] \tag{7}$$

where ϕ is a real function and A is a slow varying real function of x and y. In order to satisfy (4), we require ϕ and A to satisfy the following equations:

$$\nabla\phi \cdot \nabla\phi = 1 \tag{8a}$$

$$\nabla \cdot (A^2 \nabla\phi) = 0 \tag{8b}$$

where $\nabla^2 A / k_0^2 n_e^2 A$ is assumed to be approximately zero. Clearly $\nabla\phi$ is perpendicular to the wave front surface defined by ϕ = constant. If we compute the time-averaged Poynting vector of ψ, it is proportional to $A^2 \nabla\phi$. Thus (8b) is a statement of conservation of energy in the guided-wave beam. Substituting (7) into (3a) and (6b) and neglecting the term $\nabla A / (jk_0 n_e A)$ with respect to $\nabla\phi$ because of the slow variation of A, we obtain

$$\boldsymbol{E}_E = A \exp(-jk_0 n_e \phi) F_E (\boldsymbol{i}_z \times \nabla\phi) \tag{9}$$

$$\boldsymbol{E}_M = A \exp(-jk_0 n_e \phi) \cdot \left\{\left[\frac{F_M \nabla\phi \cdot \nabla\phi}{\epsilon(z)}\right] \boldsymbol{i}_z - \frac{j}{k_0 n_e \epsilon(z)} \frac{\partial F_M}{\partial z} \nabla\phi\right\}. \tag{10}$$

B. The Vector Wave Equation Including the Grating

When there is a grating structure on a single-mode isotropic planar waveguide, the ϵ variation in (1) is much more complicated. It must include the deviation of dielectric constant caused by the grating. If we include the variations of ϵ and the effect of waveguide attenuation, we obtain

$$k_0^2\epsilon = k_0^2[\epsilon(z) + W(x, y)\Delta\epsilon(z)\epsilon'(x, y)] - 2jk_0 n_e \alpha \tag{11a}$$

where α is the waveguide attenuation coefficient that may be determined experimentally [11]. α typically consists of the loss due to waveguide material and the radiation loss due to random scattering loss by the defects. $\epsilon'(x, y)\Delta\epsilon(z)$ is the deviation of the dielectric constant from the $\epsilon(z)$ of the planar waveguide produced by the grating. $W(x, y)$ is the window function that defines the shape of the grating region, $W(x, y) = 1$ inside the grating region and $W(x, y) = 0$ outside the grating region. We have also assumed that the deviation of the dielectric constant caused by the grating can be described by a z variation of $\Delta\epsilon$ multiplied by an x and y variation of ϵ'. This assumption is strictly valid only for gratings with rectangular groove profiles. In order to demonstrate our analytical method, we will further assume

$$\epsilon' = g\cos[\Gamma(x, y)] + \text{higher order terms} \tag{11b}$$

where g is a constant, the higher order terms are neglected, and $\Gamma(x, y)$ describes the quasi-periodic variation of Λ. When the grating is strictly periodic, this approximation is equivalent to expanding the ϵ' in Fourier series and approximating the ϵ' by its first Fourier term. In a quasi-periodic structure with large chirping rate and/or curvature, this approximation may not be very accurate and the higher order terms may need to be taken into account.

C. The Two-Dimensional Generalized Coupled-Mode Equation

Our task is to simplify (1) to a coupled-mode equation with the ϵ given by (11a). In the case involving two TE beams, we assume that the total electric field is given by the summation of the two interacting TE guided-wave

beams

$$\boldsymbol{T}_E = P(x,y)A_1\exp(-jk_0n_e\phi_1)F_E(\boldsymbol{i}_z\times\nabla\phi_1) + Q(x,y)A_2\exp(-jk_0n_e\phi_2)F_E(\boldsymbol{i}_z\times\nabla\phi_2). \quad (12)$$

Let us consider first both the incident and diffracted beams which are specified such that A_1, A_2, ϕ_1, and ϕ_2 satisfy (8). P and Q are unknown complex slow varying functions of x and y. Since A_1, A_2, ϕ_1, and ϕ_2 have already been specified, the magnitude and phase of P and Q determine the amplitude and phase of the incident and diffracted beams. Let us now substitute (11) and (12) into (1) and assume $W(x, y)$ to be a window with a very large size. Q will have large amplitude only when

$$\phi_2 = \phi_1 - (\Gamma/k_0n_e). \quad (13)$$

Equation (13) is the generalized phase matching condition of the volume interaction. It is used to determine the $\Lambda(x, y)$ that will produce the highest diffraction efficiency between the two given beams.

Let us consider next a grating structure of a given Γ that had already been designed and fabricated such that (13) is satisfied within a finite region where $W=1$. Equation (1) can be simplified in this region by substituting (13) into it and by equating the terms that have similar exponential spatial variations. We will also neglect the terms containing second derivatives of the functions P and Q. After such simplification, as illustrated in the Appendix, we obtain

$$\nabla P\cdot\nabla\phi_1+\alpha P+j\frac{A_2}{A_1}K_E(\nabla\phi_1\cdot\nabla\phi_2)Q=0 \quad (14a)$$

$$\nabla Q\cdot\nabla\phi_2+\alpha Q+j\frac{A_1}{A_2}K_E(\nabla\phi_1\cdot\nabla\phi_2)P=0 \quad (14b)$$

and

$$K_E=\frac{k_0g\int_{-\infty}^{+\infty}\Delta\epsilon(z)F_E^*F_E\,dz}{4n_e\int_{-\infty}^{+\infty}F_E^*F_E\,dz}. \quad (15)$$

Equation (14) is the generalized coupled-mode equation for the phase matched interaction of two TE beams within the chirped or the curved grating region. Notice that $\nabla\phi_1$ and $\nabla\phi_2$ are parallel to the direction of propagation of the incident and diffracted beams. Thus $\nabla\phi_1\cdot\nabla\phi_2$ expresses the degradation effect of the coupling coefficient when the polarizations of the incident and diffracted beams become significantly different from each other. This is the case of the coupled-mode equation with perfect phase matching.

Consider next the case where ϕ_1 of the incident TE beam is changed slightly; for example, the incident beam may have altered its direction of propagation. Alternatively, the Γ of the fabricated grating may be slightly different than the Γ that was designed to match ϕ_1 and ϕ_2 that are solutions of (8a). In order to calculate Q for this situation, we shall assume again the total electric field is given by (12). A_1 and ϕ_1 still satisfy (8). However, we shall now only choose A_2 to satisfy (8b), and we shall let ϕ_2 be determined by (13). ϕ_2 determined in this manner generally may not satisfy (8a). The equation equivalent to (14) obtained from (1) is now

$$\nabla P\cdot\nabla\phi_1+\alpha P+j\frac{A_2}{A_1}K_E(\nabla\phi_1\cdot\nabla\phi_2)Q=0 \quad (16a)$$

$$\nabla Q\cdot\nabla\phi_2+\alpha Q+j\frac{A_1}{A_2}K_E\frac{\nabla\phi_1\cdot\nabla\phi_2}{\nabla\phi_2\cdot\nabla\phi_2}P - \frac{k_0n_e[1-(\nabla\phi_2\cdot\nabla\phi_2)]Q}{2j}=0. \quad (16b)$$

Equation (16) corresponds to the coupled-mode equation with phase mismatch, while (14) corresponds to the coupled-mode equation without any phase mismatch. Clearly, if the value of $\nabla\phi_2\cdot\nabla\phi_2$ is very different than unity, the magnitude of Q will be small. Thus $1-\nabla\phi_2\cdot\nabla\phi_2$ is a measure of the phase mismatch.

Similarly for the case of two TM beams, the total electric field is

$$\boldsymbol{T}_M = P(x,y)A_1\exp(-jk_0n_e\phi_1)\cdot\left\{\frac{F_M}{\epsilon(z)}\boldsymbol{i}_z-\frac{j}{k_0n_e\epsilon(z)}\frac{\partial F_M}{\partial z}\nabla\phi_1\right\} + Q(x,y)A_2\exp(-jk_0n_e\phi_2)\cdot\left\{\frac{F_M(\nabla\phi_2\cdot\nabla\phi_2)}{\epsilon(z)}\boldsymbol{i}_z-\frac{j}{k_0n_e\epsilon(z)}\frac{\partial F_M}{\partial z}\nabla\phi_2\right\}. \quad (17)$$

Substituting (11) and (17) into (1) and utilizing (13), we obtain

$$\frac{1}{2}\left(1+\frac{N_M}{n_e^2}\right)\frac{\nabla P\cdot\nabla\phi_1}{\nabla\phi_2\cdot\nabla\phi_2}+\frac{\alpha P}{\nabla\phi_2\cdot\nabla\phi_2}+j\frac{A_2}{A_1}K_MQ=0 \quad (18a)$$

$$\frac{1}{2}\left(1+\frac{N_M}{n_e^2}\right)\nabla Q\cdot\nabla\phi_2+\alpha Q+j\frac{A_1}{A_2}\frac{K_MP}{\nabla\phi_2\cdot\nabla\phi_2} - \frac{k_0n_e[1-(\nabla\phi_2\cdot\nabla\phi_2)]}{2j}Q=0 \quad (18b)$$

where

$$K_M=\frac{k_0g\int_{-\infty}^{+\infty}\Delta\epsilon(z)F_M^*F_M\,dz}{4n_e\int_{-\infty}^{+\infty}F_M^*F_M\,dz} \quad (19a)$$

$$N_M=\frac{\int_{-\infty}^{+\infty}\epsilon(z)F_M^*F_M\,dz}{\int_{-\infty}^{+\infty}F_M^*F_M\,dz}. \quad (19b)$$

Equation (18) is the generalized coupled-mode equation for the interaction of two TM beams within the region of the chirped or curved grating.

In isotropic single mode planar waveguides, when the directions of propagation of incident and diffracted beams are approximately either parallel or antiparallel to each other, we expect very little interaction, i.e., mode conversion, between a TE and a TM guided wave. Thus either

(16) or (18) is applicable, depending on the polarization of the incident beam.

III. Examples of Generalized Phase-Matched Diffraction

Equation (13) is very useful in determining the $\Lambda(x, y)$ that must be used to obtain phase cumulative diffraction from a given incident beam into a given diffracted beam. For example, let the incident beam be a plane guided wave propagating in the $+x$ direction so that A_1 is a constant and $\phi_1 = x = r\cos\theta$. Let the desired diffracted beam be a cylindrical beam convergent toward the origin so that $A_2 = \text{constant}/\sqrt{r}$ and $\phi_2 = -r$ at large r. Then according to (13), $\Gamma = k_0 n_e r(1+\cos\theta)$. The loci of $\cos\Gamma = 1$ is $r(1+\cos\theta) = 2m\pi/k_0 n_e$ where m = integers. The grating groove corresponding to any specific m is just a parabola in the x, y plane with $r = 2r_0/(1+\cos\theta)$ where $r_0 = m\pi/k_0 n_e$. Fig. 2(a) illustrates such a grating pattern. Notice that in the region near the x axis, the grating grooves are approximately circular with a radius of curvature, $R \cong 2r_0$.

Consider next the case of a linear chirped grating as shown in Fig. 2(b) that has groove positions corresponding to $k_0 n_e \sin\theta_0(1+cy)y = m\pi$. A plane guided-wave is incident on the grating at the angle θ_i. In this case

$$\Gamma = 2k_0 n_e \sin\theta_0(1+cy)y$$

and

$$\phi_1 = \cos\theta_i x + \sin\theta_i y.$$

We can calculate ϕ_2 from (13) to obtain

$$\phi_2 = \phi_1 - \frac{\Gamma}{k_0 n_e} = \cos\theta_i x + \sin\theta_i y - 2\sin\theta_0(1+cy)y$$

where

$$c = 1/(4X\tan\theta_0)$$

X is the focal length. From the calculated ϕ_2 we conclude that for small $|x|$ values, the diffracted beam is a convergent beam focused on the focal point at $x = X$, $y = -X\tan\theta_i$ when $\theta_i = \theta_0$. Here, ϕ_2 does not satisfy (8a). The amplitude of the diffracted beam will be very small unless $\nabla\phi_2 \cdot \nabla\phi_2 \sim 1$. Since the value of $\nabla\phi_2 \cdot \nabla\phi_2$ deviates significantly from unity when $|y|$ is large, the linearly chirped grating lens is efficient only for relatively slow chirping rate.

If we want to obtain high efficiency for a chirped grating that has large chirping rate and small K_E (or K_M) values, the length of the grating should be long. We also need to use a grating such that the ϕ_2 obtained from that Γ will satisfy (8a) over the entire grating area. In that case, we must use curved chirped gratings as illustrated in Fig. 2(c). In this figure, the boundaries of the window function are illustrated by the rectangular box. If the grating grooves were extended outside of the window boundary, two typical loci of the extended grating grooves are as shown by the dashed curves in Fig. 2(c).

In short, equation (13) is useful in two ways: a) to find the desired grating groove shape for a given set of desired incident and diffracted beams; and b) to calculate ϕ_2 and to estimate approximately the effectiveness of the diffraction by calculating $\nabla\phi_2 \cdot \nabla\phi_2$ for a given grating and a given incident beam.

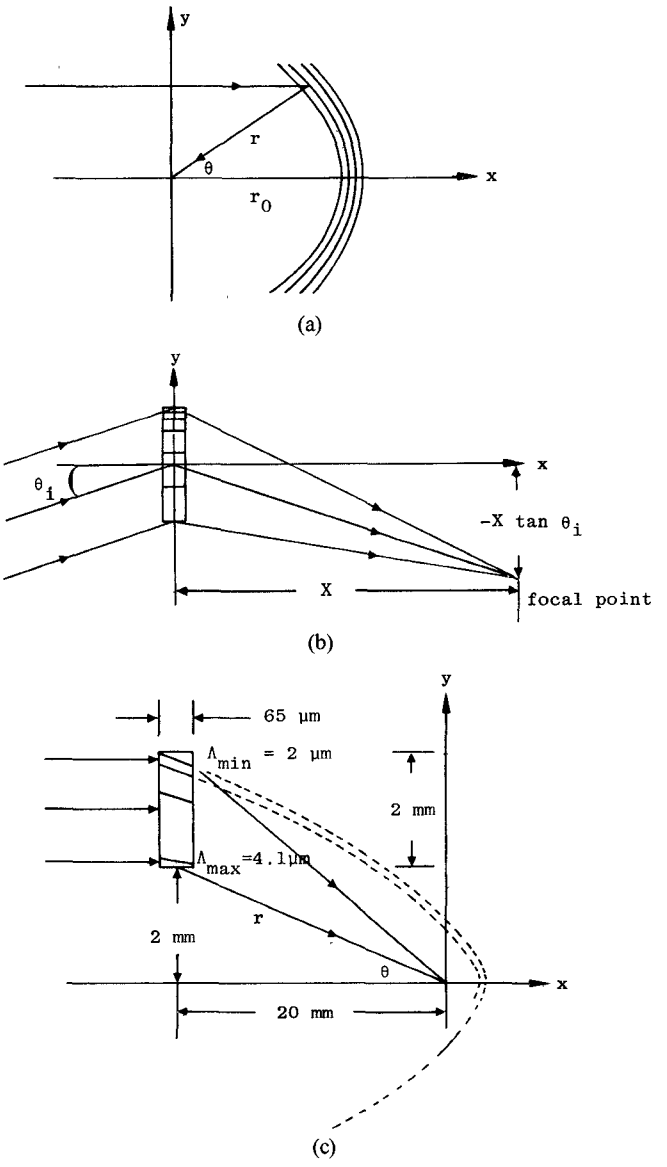

Fig. 2. Examples of diffraction of guided-wave beams by chirped or curved gratings.

IV. Solutions of the Coupled-Mode Equation

If either P or Q is eliminated from (16) or (18), we will obtain a second-order differential equation. The available analytical solutions for such a second-order differential equation are, in general, very limited. Solymar has obtained an analytical solution for the special case of a plane wave interacting with a cylindrical wave without any phase mismatch [13]. We have developed here a general method for integrating numerically (16) and (18) along the Eikonal lines. In addition, we will also establish the boundary conditions at the edge of the window area to initiate the numerical procedure.

Let us define an Eikonal line of the incident wave as a curve that is tangent to the direction of propagation of the

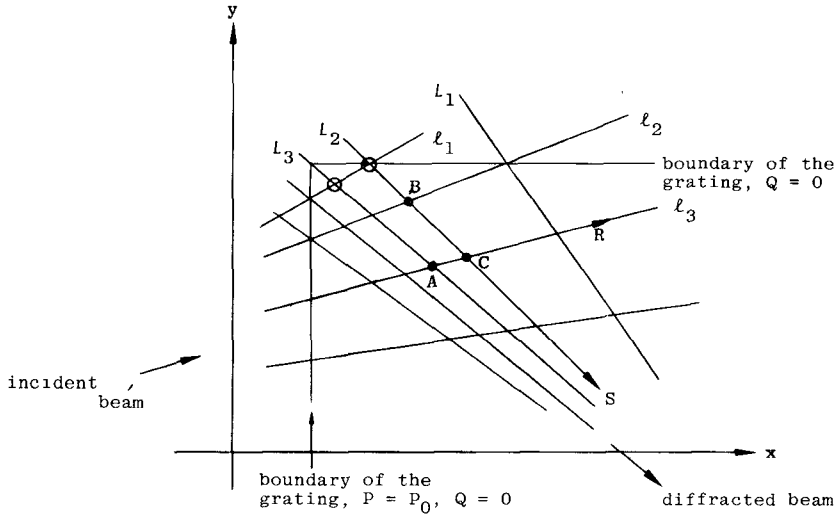

Fig. 3. Illustration of Eikonal lines and the boundary conditions.

incident wave and that follows the propagation of the incident wave passing through a given point. Thus, the Eikonal line is always parallel to $\nabla\phi_1$. The magnitude of $\nabla\phi_1$ is unity. Hence

$$\nabla P\cdot\nabla\phi_1 = dP/dR \tag{20}$$

where dR is the incremental distance along the Eikonal line. Several Eikonal lines of the incident beam are illustrated as $l_1, l_2, l_3, \cdots$ in Fig. 3. Similarly, along the Eikonal line of the diffracted beam marked as $L_1, L_2, \cdots$ in Fig. 3, we obtain

$$\nabla Q\cdot\nabla\phi_2 = (dQ/dS)(\nabla\phi_2\cdot\nabla\phi_2)^{1/2}. \tag{21}$$

Here the magnitude of $\nabla\phi_2$ is included explicitly in (21) because it is not necessarily unity, and dS is the incremental distance along the Eikonal line of the diffracted beam. The slope of the Eikonal lines for the incident and diffracted beams is

$$\tan\theta_R = (\nabla\phi_1\cdot\boldsymbol{i}_y)/(\nabla\phi_1\cdot\boldsymbol{i}_x) \tag{22a}$$

$$\tan\theta_S = (\nabla\phi_2\cdot\boldsymbol{i}_y)/(\nabla\phi_2\cdot\boldsymbol{i}_x). \tag{22b}$$

Substituting (20) and (21) into (16), we obtain

$$\frac{dP}{dR} = -\alpha P - \frac{A_2}{A_1} jK_E(\nabla\phi_1\cdot\nabla\phi_2)Q \tag{23a}$$

$$j(\nabla\phi_2\cdot\nabla\phi_2)^{1/2}\frac{dQ}{dS} = \frac{A_1}{A_2}K_E P\frac{\nabla\phi_1\cdot\nabla\phi_2}{\nabla\phi_2\cdot\nabla\phi_2} - j(\alpha+j\xi)Q \tag{23b}$$

where

$$\xi = k_0 n_e[1-\nabla\phi_2\cdot\nabla\phi_2]/2.$$

Equation (23a) implies that along a given Eikonal line l_3, the value of P at C (which is located at $R=R_c$ and $S=S_c$ on the Eikonal lines l_3 and L_2) can be calculated numerically in terms of the value of P and Q at A for a small R_C-R_A value by the Taylor series expansion. Similarly, equation (23b) implies that the value of Q at C can be expressed in terms of the value of P and Q at B for a small S_C-S_B value by the Taylor series expansion. Mathematically, for the TE beams, equation (23) can be rewritten into the form of a difference equation

$$P(R_C)-P(R_A)\exp[-\alpha(R_C-R_A)] = -\frac{A_2}{\alpha A_1}K_E(\nabla\phi_1\cdot\nabla\phi_2)jQ(R_A)\cdot\{1-\exp[-\alpha(R_C-R_A)]\} \tag{24}$$

$$jQ(S_C)-jQ(S_B)\exp(-\gamma) = \frac{A_1}{A_2}K_E\frac{\nabla\phi_1\cdot\nabla\phi_2}{\nabla\phi_2\cdot\nabla\phi_2}P(S_B)\frac{[1-\exp(-\gamma)]}{(\alpha+j\xi)} \tag{25}$$

where

$$\gamma = (\alpha+j\xi)(S_C-S_B)/(\nabla\phi_2\cdot\nabla\phi_2)^{1/2}.$$

Here, we have assumed that A, B, and C are points within the boundary of the window function and that the change of $(\nabla\phi_2\cdot\nabla\phi_2)$, ξ, P, and Q from point A to C and from point B to C is so small that the contribution due to their variation to the right hand side of (24) and (25) is negligible. A set of equations similar to (24) and (25) can be obtained for TM beams based on (18).

Our numerical procedure begins with the boundary conditions at the edge of the window function. In terms of the boundary lines illustrated in Fig. 3, we use $P=P_0$ and $Q=0$ on the boundary line. This assumption is reasonable because the incident beam has just reached the grating. We use $Q=0$ with unknown P on the upper boundary line because the diffracted beam has just initiated at that edge of the grating region. We will set up a mesh consisting of a set of Eikonal lines L_j intersecting a set of Eikonal lines l_k. The spacing of the mesh points is determined by the desired accuracy of the numerical results. We will first

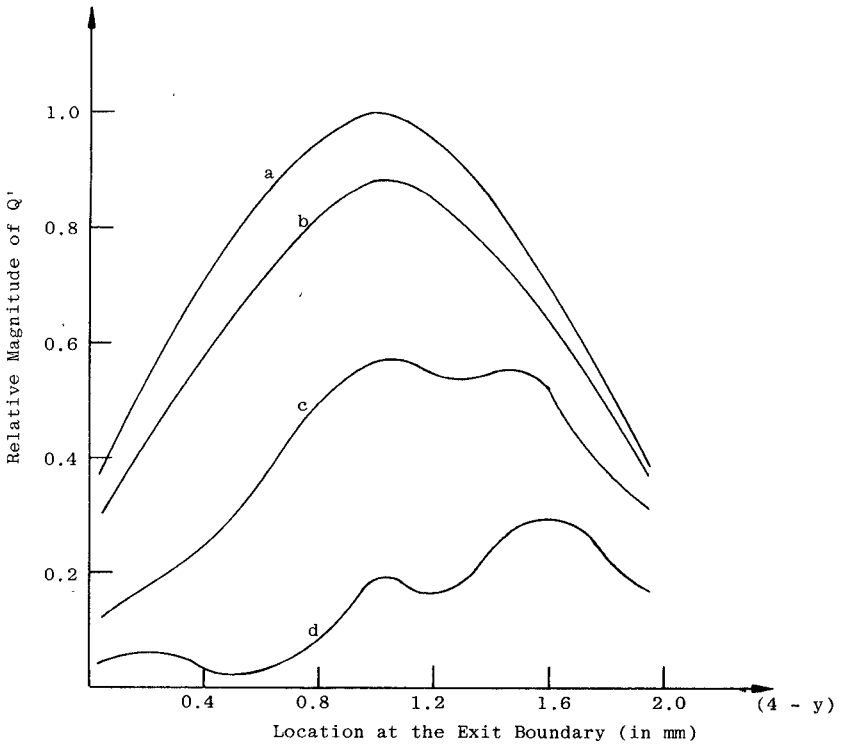

Fig. 4. Calculated amplitude distribution of diffracted wave at the exit boundary of the grating region.

compute the Q values of the set of mesh points along each l_k Eikonal line in terms of the boundary value on the $P=P_0$, $Q=0$ boundary followed by the computation of the P values of these mesh points. This first set of mesh points is indicated by circles in Fig. 3. The position of each mesh point is calculated by solving the simultaneous equations

$$y_C - y_A = \tan\theta_R (x_C - x_A)$$

$$y_C - y_B = \tan\theta_S (x_C - x_B)$$

where (x_C, y_C) is the position of the mesh point to be calculated and (x_A, y_A) and (x_B, y_B) are the known positions of the mesh points calculated previously or on the boundary. $\tan\theta_R$ and $\tan\theta_S$ are given by (22). This process is repeated for the set of mesh points adjacent to the set of mesh points where P and Q values have just been calculated. The final set of mesh points are the points of the intersection of the Eikonal lines with the exit boundary of the window function W.

V. Numerical Results from a Selected Example

Although this method has been applied by us to calculate the performance of many devices such as the curved grating lens, linear chirped grating lens, curved chirped grating reflector, etc., the demonstration of this method will only be presented here by showing the numerical results obtained in a specific example. In this example, we calculate the curved chirped grating lens diffracting an incident Gaussian guided-wave beam into a focused guided-wave beam with a focal point at $x=0$, $y=0$, as illustrated in Fig. 2(c). In this case

$$A_1 = 1$$

$$\lambda = 0.6328\times 10^{-6}\ \text{m}$$

$$W = [u(y-0.002) - u(y-0.004)] \cdot [u(x+20.0325\times 10^{-3}) - u(x+19.9675\times 10^{-3})]$$

$$P_0 = 1.293 \exp\left[-(y-3\times 10^{-3})^2 \cos^2\theta_i / 10^{-6}\right]$$

$$A_2 \doteq 1/r^{1/2}$$

$$\phi_1 = \cos\theta_i x + \sin\theta_i y$$

$$\Gamma = k_0 n_e r(1+\cos\theta)$$

$$\alpha = 10\ \text{m}^{-1}$$

where u is a unit step function, $u(v)=0$ for $v<0$ and $u(v)=1$ for $v\geq 0$. We have used a $\epsilon(z)$ and $\Delta\epsilon(z)$ for a glass waveguide such that $n_e=1.53$ and $K_E=0.024$, μm^{-1} and we have chosen the Eikonal lines to be approximately 1 μm apart.

Fig. 4 shows the calculated value of the amplitude of Q at the exit boundary, $x=-19.9675\times 10^{-3}$ m and $0.002<y<0.004$ m, for four different cases, $\theta_i=0$ in case a, $\theta_i=0.01$ radian in case b, $\theta_i=0.02$ radian in case c, and $\theta_i=0.03$ radian in case d. Fig. 5 shows the calculated phase of jQ at the same boundary. Notice that the phase of jQ for case a is always zero because the grating is designed to provide perfect phase match for that case. As the θ_i is deviated further away from the phase matched condition, the phase

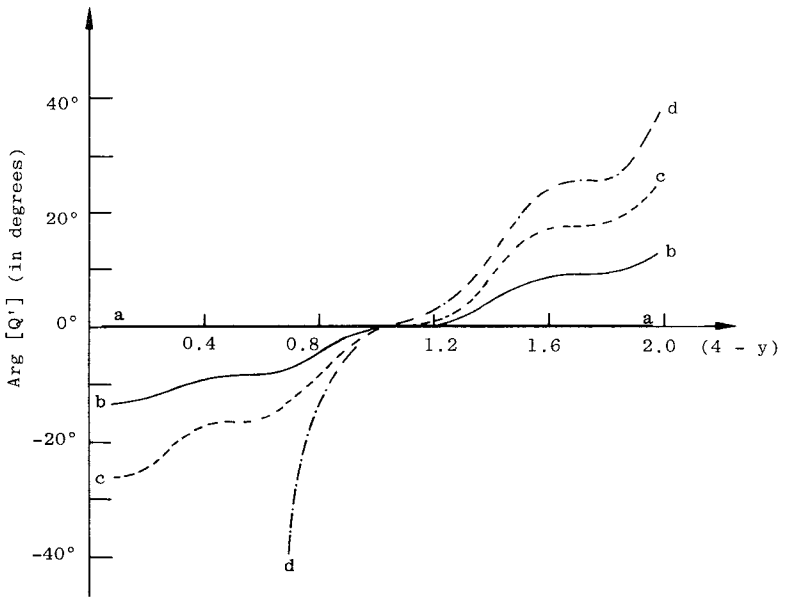

Fig. 5. Calculated phase deviation of the diffracted wave at the exit boundary of the grating region.

of jQ changes much more rapidly. Figs. 6 to 9 show the calculated amplitude of the electric field as a function of y in the $x=0$ plane, i.e., the focal plane. Such an electric field has been calculated by means of the Kirchhoff's diffraction integral using the Fresnel approximation. Notice the degradation of the diffracted pattern as the θ_i moves away from the phase matching angle.

VI. Discussion

We have presented in this paper a generalized two-dimensional coupled-mode analysis of two generalized guided-wave beams in a planar waveguide coupled by a chirped and curved grating. From this analysis, we have obtained the generalized phase matching condition that can be used to design the grating groove shape for any two given guided-wave beams. Alternatively, we can use the coupled-mode equation to calculate the phase and amplitude distributions of the two beams when there is a phase mismatch. From the calculated amplitude and phase distribution, we can obtain information such as the diffracted field patterns, the diffraction efficiency, the angular range of the incident beam propagation within which effective diffraction can take place, the effect of changing the beam shape of the incident beam (e.g., a Gaussian beam instead of a plane wave), and the effect of changing the grating parameter (e.g., changing the K coefficient or the curvature).

However, this analysis has several limitations. First, we have confined our analysis to the case of a single mode waveguide with negligible radiation loss. Secondly, only a limited amount of mismatch can be handled by this analysis. This is because we have considered the amplitude functions P and Q to be slow varying functions within a wavelength of the guided mode, so that terms containing the second derivatives of P and Q can be neglected in (16) and (18). It can be shown that the second derivatives of P and Q are negligible whenever $[1-(\nabla\phi_2\cdot\nabla\phi_2)]\ll 1$. In most cases, this is not a severe restriction. In all the examples of the grating lens that we have calculated so far, $[1-(\nabla\phi_2\cdot\nabla\phi_2)]$ has not exceeded 10^{-2}. On the other hand, we have found that the condition for negligible excitation of the substrate radiation mode by the chirped grating structure is often violated before the violation of this condition.

This analysis has already been applied to calculate the performance of Fresnel and chirped grating lenses. Experimental work to verify the calculated results is currently being undertaken in our laboratory. It will be published elsewhere.

Appendix A: Mathematical Steps in the Derivation of the Coupled-Mode Equation

From (2), (5), (8b), (9), and (10), we obtain

$$\{\nabla\times\nabla\times[P(x,y)\boldsymbol{E}_E]\}\cdot\boldsymbol{i}_E = [Pk_0^2\epsilon(z)-Pk_0^2n_e^2(1-\nabla\phi\cdot\nabla\phi) +2jk_0n_e(\nabla P\cdot\nabla\phi)]E_E \tag{A1}$$

$$\{\nabla\times\nabla\times[P(x,y)\boldsymbol{E}_M]\} = \left[Pk_0^2\epsilon(z)-Pk_0^2n_e^2(1-\nabla\phi\cdot\nabla\phi) +j\left(k_0n_e+\frac{k_0\epsilon(z)}{n_e}\right)(\nabla P\cdot\nabla\phi)\right]\boldsymbol{E}_M \tag{A2}$$

where

$$\boldsymbol{i}_E=\boldsymbol{E}_E/E_E.$$

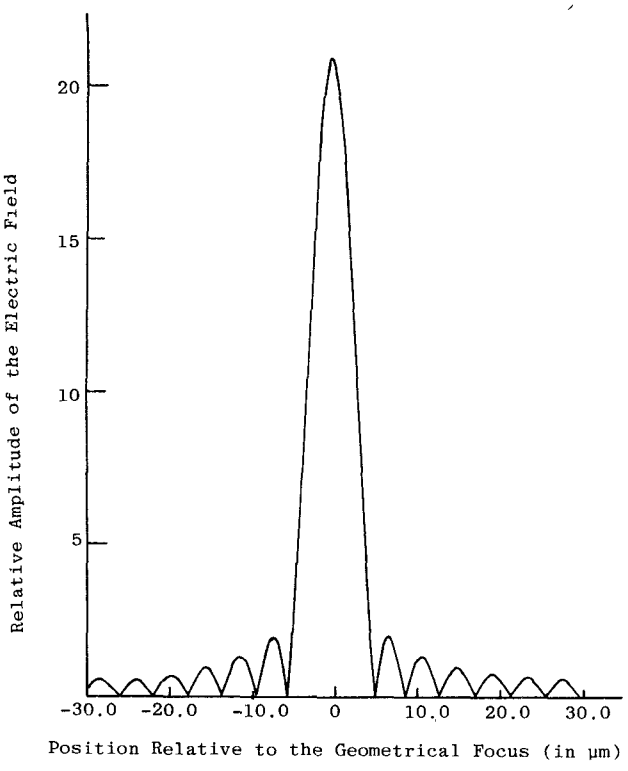

Fig. 6. Diffraction pattern in the focal plane (case a) for Gaussian beam with angle of incidence at 0 rad.

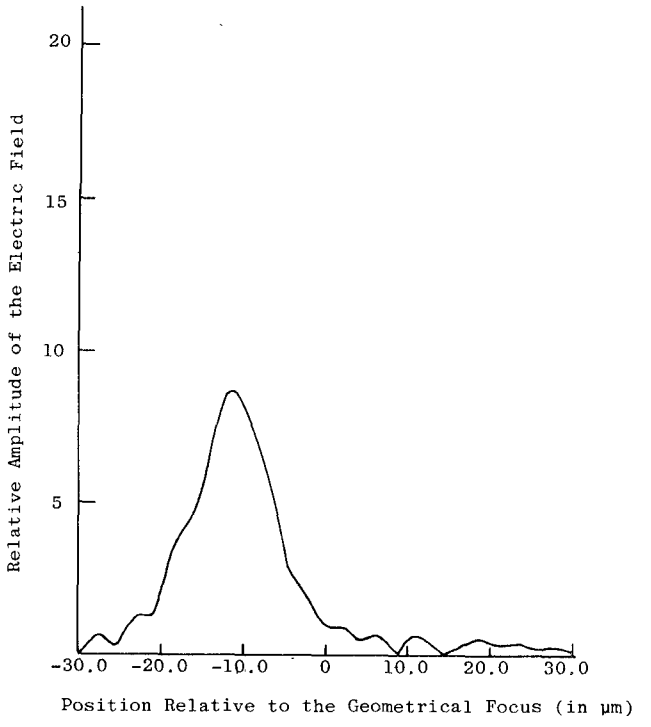

Fig. 8. Diffraction pattern in the focal plane (case c) for Gaussian beam with angle of incidence at 0.02 rad.

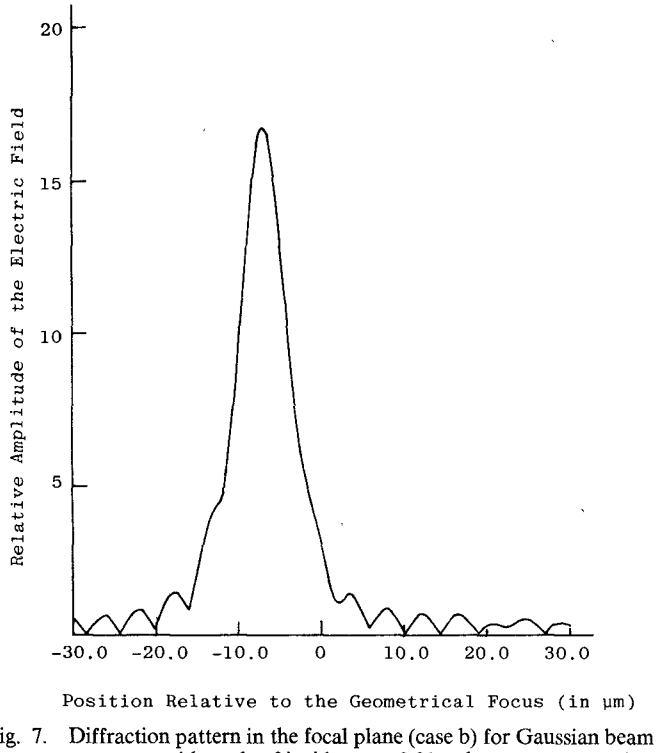

Fig. 7. Diffraction pattern in the focal plane (case b) for Gaussian beam with angle of incidence at 0.01 rad.

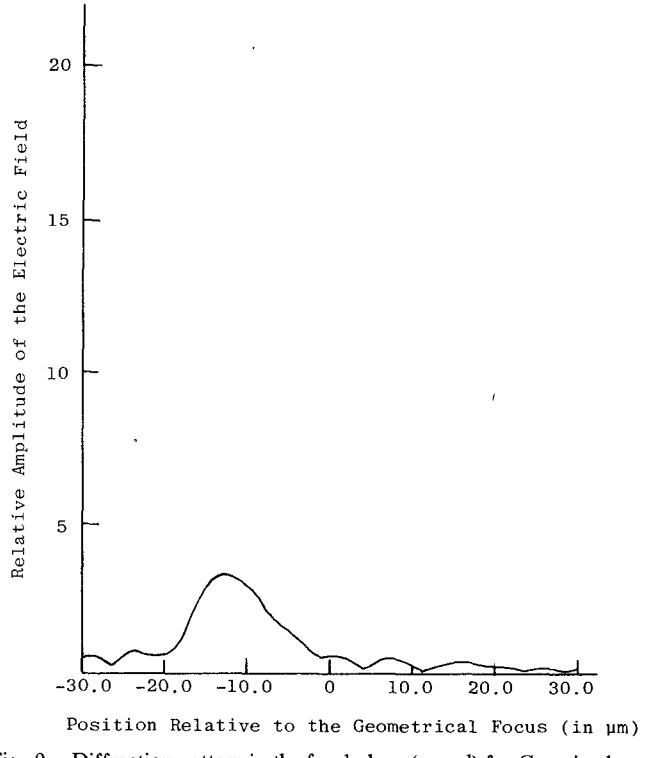

Fig. 9. Diffraction pattern in the focal plane (case d) for Gaussian beam with angle of incidence at 0.03 rad.

We have neglected terms of the magnitude of $(\nabla A/k_0 n_e A)$ and $[1-\nabla\phi\cdot\nabla\phi](dF_M/dz)/k_0 n_e F_M$. Substituting (12) into (1), making use of (13) and (A1), equating the terms that have the same x and y variations in the exponential factor, neglecting the terms containing second derivatives of functions P and Q as they are considered to

be higher order small quantities, we obtain for the generalized TE guided-wave beams

$$(\boldsymbol{i}_z \times \nabla\phi_1)(\nabla P \cdot \nabla\phi_1 + \alpha P)A_1F_E + (\boldsymbol{i}_z \times \nabla\phi_2) \cdot \left(\frac{jk_0 g}{4n_e}\right) W(x,y) Q \Delta\epsilon(z) A_2 F_E + \text{vector quantities perpendicular to } (\boldsymbol{i}_z \times \nabla\phi_1) = 0 \quad \text{(A3)}$$

$$(\boldsymbol{i}_z \times \nabla\phi_2)(\nabla Q \cdot \nabla\phi_2 + \alpha Q)A_2F_E + (\boldsymbol{i}_z \times \nabla\phi_1) \cdot \left(\frac{jk_0 g}{4n_e}\right) W(x,y) P \Delta\epsilon(z) A_1 F_E + (\boldsymbol{i}_z \times \nabla\phi_2)\left(\frac{jk_0 n_e}{2}\right)[1 - \nabla\phi_2 \cdot \nabla\phi_2] Q A_2 F_E + \text{vector quantities perpendicular to } (\boldsymbol{i}_z \times \nabla\phi_2) = 0. \quad \text{(A4)}$$

Here, g is the coefficient given in (11b) and we have assumed that the size of the area within which the window function is not zero is large so that terms of the same x and y variation in the exponential factor must be equal to each other. Following Kogelnik [10] and Kenan [11], forming an inner product between the quantities in (A3) and $F_E^*(\boldsymbol{i}_z \times \nabla\phi_1)$ and integrating with respect to dz from $z=-\infty$ to $z=+\infty$, we obtain (16a) when $W(x,y)=1$. Forming an inner product between the quantities in (A4) and $F_E^*(\boldsymbol{i}_z \times \nabla\phi_2)$ and integrating with respect to dz from $z=-\infty$ to $z=+\infty$, we obtain (16b) when $W(x,y)=1$.

A similar procedure is used to derive equation (18) for the generalized TM guided-wave beams, where

$$K_M = \left\{ k_0 g \int_{-\infty}^{+\infty} \Delta\epsilon(z) \left[F_M^* F_M + \frac{1}{k_0^2 n_e^2} \left(\frac{\partial F_M^*}{\partial z}\right)\left(\frac{\partial F_M}{\partial z}\right) \nabla\phi_1 \cdot \nabla\phi_2 \right] dz \right\} \Big/ \left\{ 4n_e \int_{-\infty}^{+\infty} \left[F_M^* F_M + \frac{1}{k_0^2 n_e^2} \left(\frac{\partial F_M^*}{\partial z}\right)\left(\frac{\partial F_M}{\partial z}\right) \right] dz \right\}.$$

As the second term is much smaller than the first term, we can use the approximate expression as given in (19a).

Acknowledgment

The Visiting Scholars wish to thank the Ministry of Education of the People's Republic of China for supporting their tenure in the United States.

References

[1] P. K. Tien, "Method of forming novel curved line gratings and their use as reflectors and resonators in integrated optics," *Opt. Lett.*, vol. 1, p. 64, 1977.
[2] S. K. Yao and D. E. Thompson, "Chirped grating lens for guided-wave optics," *Appl. Phys. Lett.*, vol. 33, p. 635, 1978.
[3] P. K. Tien and R. J. Capik, "A thin film spectrography for guided-waves," in *Tech. Dig., IEEE/OSA Topical Meet. Integrated and Guided-Wave Optics* (Incline Village, NV), 1980.
[4] G. Hatakosi and S. Tanaka, "Grating lenses for integrated optics," *Opt. Lett.*, vol. 2, p. 142, 1978.
[5] A. Katzir, A. C. Livanos, J. B. Shellan, and A. Yariv, "Chirped gratings in integrated optics," *IEEE J. Quantum Electron.*, vol. QE-13, p. 296, 1977.
[6] S. K. Yao, "Limitation of holographic grating lenses," in *SPIE Tech. Symp. Proc.*, vol. 269 (North Hollywood, CA), Feb. 1981.
[7] A. Hardy and W. Streifer, "Analysis of waveguided Gaussian beams coupled by misaligned or curved gratings," *J. Opt. Soc. Amer.*, vol. 69, p. 1235, 1979.
[8] Solymar, L., "A general two-dimensional theory for volume holograms," *Appl. Phys. Lett.*, vol. 31, p. 820, 1977.
[9] J. Van Roey and P. E. Lagasse, "Coupled wave analysis of obliquely incident waves in thin film gratings," *Appl. Opt.*, vol. 20, p. 423, 1981.
[10] H. Kogelnik, "Coupled wave theory for thick hologram gratings," *Bell Syst. Techn. J.*, vol. 48, p. 2909, 1969.
[11] R. Kenan, "Theory of diffraction of guided optical waves by thick holograms," *J. Appl. Phys.*, vol. 46, p. 4545, 1975.
[12] M. Kline and I. W. Kay, *Electromagnetic Theory and Geometrical Optics*. New York: Interscience, 1965.
[13] L. Solymar and M. P. Jordan, "Analysis of cylindrical-to-plane-wave conversion by volume holograms," *Electron. Lett.*, vol. 12, p. 142, 1976.

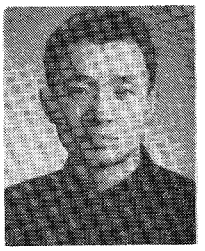

Zong-Qi Lin graduated from Jiao-Tong University, Shanghai, People's Republic of China, in 1952.

He is currently an Associate Professor in the Department of Electronic Engineering at Jiao-Tong University. Before 1962, he worked on the theory of automatic control and electronic circuits. After 1962, he was engaged in the research on electromagnetic theory and microwave engineering. At present, he is a Visiting Scholar at the University of California at San Diego, La Jolla, in the Department of Electrical Engineering and Computer Sciences.

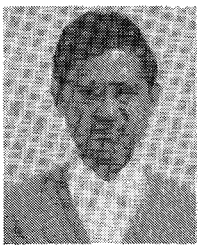

Shu-Tong Zhou was born in Shanghai, The People's Republic of China, on March 2, 1938. He graduated from Fudan University, Shanghai, The People's Republic of China, in 1961.

Currently, he is a Faculty Member of Fudan University, Shanghai, People's Republic of China. From 1961 to 1966, he did research in the field of electron spin resonance and nuclear magnetic resonance. From 1968 to 1978, he worked in the field of microwave circuits and microwave measurements. Presently, he is a Visiting Scholar at the University of California at San Diego, La Jolla, in the Department of Electrical Engineering and Computer Sciences, where his research is in the field of guided optics.

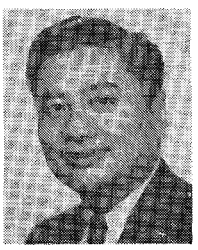

William S. C. Chang (S'56–M'58–SM'65–F'78) was born in Nantung, China, on April 4, 1931. He received the B.S. and M.S. degrees from the University of Michigan, Ann Arbor, and the Ph.D. degree from Brown University, Providence, RI, in 1952, 1953, and 1957, respectively.

He conducted research and taught at Stanford University, Stanford, CA, and the Ohio State University, Columbus, before joining the faculty of Washington University, St. Louis, MO, in 1965 as Chairman of the Electrical Engineering

Department. He later became the Samuel Sachs Professor of Electrical Engineering and the Director of the Laboratory of Applied Electronic Services. He joined the University of California at San Diego, La Jolla, as a Professor of Electrical Engineering in 1979. His research ranges from surface-wave antennas, microwave masers, lasers, hypersonic plasma, and holography to integrated optics and the use of lidar for air-pollution monitoring.

Dr. Chang is a member of the American Physical Society, the American Optical Society, and the American Society of University Professors.

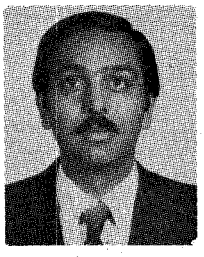

Siamak Forouhar (M'80) was born in Tehran, Iran, on August 25, 1950. He received the B.S. degree in electrical engineering from the Aryamehr Institute of Technology, Tehran, Iran, in 1972, and the M.S. degree in microwaves and modern optics from the University College, London, England, in 1975.

Since 1979, he has been working as a graduate student in the department of Electrical Engineering and Computer Sciences at the University of California at San Diego, La Jolla. He is working toward a Ph.D. degree with emphasis on the design and fabrication of grating lenses for integrated optical circuits.

Jean-Marc Delavaux (M'80) was born in Algiers, Algeria, on March 25, 1953. He received the degree of engineer from the Ecole Nationale Superieure d'Electronique, Toulouse, France, in 1978, and the M.S. degree in electrical Engineering from Washington University, St. Louis, in 1979.

Since 1979, he has been working as a graduate student in the department of Electrical Engineering and Computer Sciences at the University of California at San Diego, La Jolla. He is working toward a Ph.D. degree with emphasis on analysis and fabrication of grating lens structures.

Aperture Coupling Between Dielectric Image Lines

INDER J. BAHL, SENIOR MEMBER, IEEE, AND PRAKASH BHARTIA, SENIOR MEMBER, IEEE

Abstract—**Aperture coupling between dielectric image lines is used to develop a design technique for directional couplers at millimeter-wave frequencies. Expressions for coupling coefficients and directivity, employing coupling between image lines through apertures in the common ground plane are developed. The design procedure is illustrated by application to 10-, 20-, and 30-dB directional couplers in rectangular image lines with circular aperture coupling.**

I. Introduction

DIELECTRIC IMAGE lines and their applications in active and passive devices for millimeter-wave integrated circuits have been reported in the literature [1]–[9]. In this paper a design technique for directional couplers using dielectric image lines is given. Initially, a brief account of transmission-line properties of the dielectric image line is presented together with coupling between image lines through apertures in the common ground plane. Expressions are derived for the directivity and coupling coefficients and design curves are presented. Finally, the design procedure developed is illustrated by application to the design of 10-, 20-, and 30-dB directional couplers.

Manuscript received December 16, 1980; revised April 27, 1981. This work was supported by the Natural Sciences and Engineering Research Council of Canada under Grant A-0001.

I. J. Bahl is with the Department of Electrical Engineering, University of Ottawa, Canada K1N 6N5.

P. Bhartia is with the Defence Electronics Division, Defence Research Establishment, Ottawa, Canada K1A 0Z4.

II. Image-Line Properties

The geometry of an image line, as shown in Fig. 1, comprises a rectangular dielectric slab of relative permittivity ϵ_r backed by a perfectly conducting ground plane. The main transverse field components of the E^y_{mn} modes are E_y and H_x. Omitting the $t-z$ dependence, exp $[j(\omega t - k_z z)]$, where ω is the angular frequency and k_z is the propagation constant in the z direction; the field components inside and

0018-9480/81/0900-0891$00.75 ©1981 IEEE